Impact of new results from ultraperipheral collisions on modeling the proton and neutron emission in photon-induced nuclear processes

P. Jucha[1,*] K. Mazurek[1,†] A. Szczurek[1,2,‡] and K. Pysz[1,§]

[1]*Institute of Nuclear Physics PAN, ul. Radzikowskiego 152, Pl-31342 Kraków, Poland*

[2]*Institute of Physics, Faculty of Exact and Technical Sciences, University of Rzeszów, Pigonia 1 St., 35-310 Rzeszów, Poland*

(Received 29 August 2025; revised 7 November 2025; accepted 26 January 2026; published 17 February 2026)

Ultrarelativistic collisions of heavy ions provide a rich spectrum of possibilities to discuss the response of the nucleus to photons. Newly published neutron and proton multiplicities measured in the ALICE experiment in ultraperipheral collisions allow us to investigate the influence of the electromagnetic fields on colliding nuclei for the $^{208}\mathrm{Pb}+{}^{208}\mathrm{Pb}$ at $\sqrt{s_{NN}}=5.02$ TeV. The theoretical predictions are done within a hybrid model including equivalent photon approximations, GiBUU modeling of preequilibrium processes, and generation of the excited nuclear remnants, where decay is modeled by a statistical approach: GEM2 or GEMINI++. The cross sections of the mass-charge distributions of nuclear remnants as well as the neutron, proton, and other charged particle multiplicities are estimated. We concentrate on production of protons and isotopes coming from the electromagnetic dissociation. Special attention is devoted to emission of a single proton. It is explained in the paper that cross section for $1p$ emission is very close to maximal available one based on reactions of photon with individual nucleons (protons or neutrons) inside the nucleus.

DOI: 10.1103/nds6-c3kv

I. INTRODUCTION

The particle multiplicities are one of the basic observables measured in many low- and high-energy collision experiments. In ultrarelativistic heavy-ion reactions this observable is not straightforward as the emitted particles go in very forward or very backward directions. The multiplicity of neutrons in ultraperipheral collisions (UPC) of $^{208}\mathrm{Pb}$ + $^{208}\mathrm{Pb}$ published by the ALICE Collaboration [1] was successfully described in Refs. [2,3]. For this purpose the photon flux was calculated using the equivalent photon approximation (EPA) [4]. To calculate the photon interaction with the nuclear system, the phenomenological two-component model (TCM) [2] was proposed. In this approach the excitation of a nucleus induced by absorption of (single or multiple) photons has been assumed to be a combination of two exponential functions with one free parameter. The remnant of the photon-nucleus interaction with calculated in this way excitation energy has been further processed with statistical models EMPIRE [5], GEMINI++ [6], and HIPSE [7] and their combinations. Theoretical neutron multiplicities were obtained from the combination of these models.

The best agreement with the ALICE data was observed for simulations with a simple model proposed by us called TCM + GEMINI++. The details of the photon-nucleus collision process and the energy released during the intranuclear cascade as a kinetic energy in preequilibrium emission of neutrons and other particles were disregarded in the model.

Recently, the ALICE collaboration presented also results for proton emission [8] based on the use of so-called proton zero-degree calorimeters (ZDC). As will be discussed in our paper the new results shed new light on nuclear photoproduction processes.

The present work extends previous considerations by including a microscopic description of the photon-nucleus collision process for photon energy above 200 MeV. This approach gives insight into yields of preequilibrium emission of nucleons and pions, and thus an explicit distribution of excitation energies of UPC remnants. The fate of the latter can be examined with the deexcitation models for thermalized nuclei.

While in the previous paper [2,3] the contribution of low-energy component of photon flux (below 200 MeV) was examined, here the emphasis is put on the contribution of photons with energies extending from 200 MeV to almost 1 TeV. In summary, the hybrid model discussed here consists of three main parts as follows:

(1) Calculation of the photon flux surrounding the colliding Pb nucleus (EPA model).

(2) Estimation of photon-Pb interaction in the preequilibrium phase by excitation energy of remnants and mass-charge distribution of the hot spectator (TCM or HIPSE for energy

*Contact author: Pawel.Jucha@ifj.edu.pl
†Contact author: Katarzyna.Mazurek@ifj.edu.pl
‡Contact author: Antoni.Szczurek@ifj.edu.pl
§Contact author: Krzysztof.Pysz@ifj.edu.pl

Published by the American Physical Society under the terms of the Creative Commons Attribution 4.0 International license. Further distribution of this work must maintain attribution to the author(s) and the published article's title, journal citation, and DOI. Funded by SCOAP³.

range 20–200 MeV and GiBUU for more energetic γ rays, $E_\gamma > 200$ MeV).

(3) Deexcitation of the collision remnants created in a preequilibrium phase, with the help of models: GEM2 or GEMINI++ to obtain the particle multiplicities and mass-charge distribution of the final products.

The paper is organized as follows: The details of the theoretical approaches used are shown in Sec. II; in Sec. III results for mass-charge distribution of Pb remnants as well as the neutron and proton multiplicity are presented. Section IV contains a comparison of the obtained results with the data measured by the ALICE experiment and a detailed discussion of the processes participating in the total cross section in photon-nucleus collisions. The conclusions based on the data close the paper.

II. THEORETICAL MODELS

A. Equivalent photon approximation model and photon flux

The electromagnetic interaction caused by moving charged nuclei generates the photon flux, which is calculated using the EPA [4]. The analytic formula for a pointlike nucleus could be written as, e.g., in Ref. [9]:

$$N(\omega, b) = \frac{\alpha Z^2}{\pi^2}\frac{u^2}{\beta^2\omega b^2}\left(K_1^2(u) + \frac{1}{\gamma^2}K_0^2(u)\right). \quad (1)$$

For extended charge, one has

$$N(\omega, b) = \frac{Z^2\alpha_{\rm em}}{\pi^2\beta^2}\frac{1}{\omega b^2} \times \left|\int d\chi\ \chi^2 \frac{F\left(\frac{\chi^2+u^2}{b^2}\right)}{\chi^2+u^2} J_1(\chi)\right|^2. \quad (2)$$

Above ω is photon energy and b is transverse distance of photons from the emitting nucleus. The photon energy in the rest frame of the absorbing nucleus gives $\omega = E_\gamma$. In the case of our reaction we need a characteristics of the fluxes in the rest frame of the target nucleus. At the LHC energies $\beta \approx 1$. Since γ is very large, the second term in Eq. (1) practically vanishes. The electromagnetic form factor of the nucleus $F(\frac{\chi^2+u^2}{b^2})$ depends on $u = \frac{\omega b}{\gamma\beta}$, $\gamma = \frac{1+\beta^2}{1-\beta^2}$, χ is an auxiliary dimensionless variable related to the photon transverse momentum via the relation $\chi = k_\perp b$. In the realistic case $F(\frac{\chi^2+u^2}{b^2})$ is calculated as a Fourier transform of the nucleus charge density.

The EPA method allows us to estimate the impact parameter space distribution of photons produced by fast moving charged sources. In Eq. (2), $N(\omega, b)$ means rather $\frac{dN(\omega,b)}{d\omega d^2b}$ to shorten other more complicated formulas. Photons are typically produced with energies below 20 MeV, but there is a sizable probability of generating highly energetic γ rays. This energetic quasireal photons appear for the intranuclear impact parameter $b = R_{A_1} + R_{A_2} > 14$ fm, where UPC take place. The partner nucleus absorbs such photons and gets excited. The excitation energy range is typical for nuclear processes such as γ-ray and particle emission, fission, or even multifragmentation. Excitation of low-mass nucleon resonances can be involved.[1]

B. Models of collision process

Microscopic models of nuclear collisions, which include photons as a projectile, are scarce. Among them the RELDIS code has to be mentioned [10], but unfortunately it is not accessible to us. We decided to employ the broadly used GiBUU model [11]. It is a model of hadron, nucleus, and lepton collisions with various targets. Large scope of hadron physics as well as a heavy ion (HI) collision phenomena are implemented at very broad energy range. The good predictive power of GiBUU model for various fields of its implementation was verified many times (see, e.g., Refs. [12–15]).

The GiBUU model is unique because it also includes the photon-N and photon-A interaction. It is done explicitly for a real photon at low energies (below $\approx$2 GeV) and via virtual photon created in lepton interaction at higher energies.

The GiBUU model utilizes the so-called Boltzmann-Uehling-Uhlenbeck transport equation. The solution of BUU equation is performed by Monte Carlo simulations of motion of involved particles. It is done with sets of test particles, where n of test particles replace each of a reaction constituent. For the resulting distributions, the contributions from all test particles are summed up with appropriate weights.

In case of reactions where nuclei are involved, the BUU model calculations are able to produce the distributions of mesons and single nucleons, both emitted and those forming a remnant. The remnant nucleus of the intranuclear cascade can be defined by its mass, charge, energy, and excitation energy.

Due to a lack of a mechanism that allows for particle correlations, the simulation with the GiBUU must be restricted only to emission of single-nuclear products.

For the simulations with the use of GiBUU, in general, the standard parameters proposed by the authors of the model, were used [11]. However, since in the explored energy ranges two different approaches for the photon-induced reaction are demanded (real photon at low energy and virtual photon at high energy), the simulation parameters have been a bit adjusted in order to obtain a smooth transition between the low- and high-energy results. The estimated uncertainty of simulation results due to a variation in model parameters is estimated for 20%.

In our recent article [2] we showed that the excitation energy of nucleus in the equilibrium state is not equal to the absorbed photon energy. To describe this effect, we proposed a phenomenological approach called TCM. In this simple model the nucleus excitation energy is encoded in the function

$$P(E_{\rm exc}; E_\gamma) = c_1(E_\gamma)\delta(E_{\rm exc} - E_\gamma) + c_2(E_\gamma)/E_\gamma, \quad (3)$$

where $P(E_{\rm exc}; E_\gamma)$ (see Ref. [2]) is a conditional distribution in $E_{\rm exc}$ populated at a given photon energy E_γ and

$$c_1(E_\gamma) = \exp(-E_\gamma/E_0), \quad (4)$$

[1] Δ^+ or Δ^0 are the most representative examples.

$$c_2(E_\gamma) = 1 - \exp(-E_\gamma/E_0). \quad (5)$$

The E_0 parameter was set to the value of 50 MeV. Using the probabilistic formula for GEMINI++ results (see Sec. II C), one is able to describe the experimental data from photon-nucleus interactions with evaporation of a given number of neutrons [2].

The EMPIRE framework is a modular system of nuclear reaction codes. It combines various nuclear models to permit description of nuclear collisions in a broad energy range (kiloelectronvolts to hundreds of megaelectronvolts) and different incident particles (neutron, proton, light, and even heavy nuclei or photon). The code accounts for the major nuclear reaction mechanisms, including direct (ECIS03, CCFUS models) and preequilibrium (ORION + TRISTAN model). The compound nucleus is treated by NVWY multistep compound approach or by either a preequilibrium exciton model with cluster emission (PCROSS) or by another one with full angular momentum coupling (DEGAS). The compound nucleus decay is described by the full-featured Hauser-Feshbach model with γ-cascade and width fluctuations. The fission channel takes into account transmission through a multiple-humped fission barrier with absorption in the wells. The fission probability is derived in the WKB approximation using the optical model. The several data bases with experimental data or precalculated results with a microscopic model based on Hartree-Fock-Bogolyubov (HFB) single-particle level schemes with collective enhancement, nuclear masses, optical model parameters, ground-state deformations, discrete levels and decay schemes, level densities, fission barriers, moments of inertia, and γ-ray strength functions are included.

Another well-known collisions model relevant for particle+nucleus collisions is heavy-ion phase-space exploration (HIPSE) [7] devoted to intermediate energy range.

The HIPSE model describes the heavy-ion collision in several stages: from the contact point, by reaggregation of the constituents of overlapping nuclei, to deexcitation of prefragments. This last stage is performed within the state-of-the-art statistical approach GEMINI++ [6]. In general, it was used with success to describe reaction with collision energies 15–100 MeV per nucleon. The reaction $n + {}^{207}$Pb is chosen in Ref. [2], as the neutron interactions seem to be the only possible approximation of the photon interaction. Strictly speaking the HIPSE does not allow for a photon-induced reaction.

C. Deexcitation models

There exist several models, both statistical and dynamical, which describe the deexcitation of a hot rotating nucleus.

The Weisskopf-Ewing formalism [16] is used for particle evaporation from the excited nucleus in energy equilibrium in the general evaporation model (GEM2) [17,18]. The density of states is given by the Gilbert-Cameron formula [19] with modification as in the LAHET code [20]. The relevant reaction cross sections are parametrized. The kind of particles emitted is determined by sampling its probability distribution. Coulomb barrier is taken into account. The emission of both the stable as well as the excited ejectiles is considered. The angular distribution of emitted ejectiles is isotropic in the center-of-mass system of the parent nucleus. The angular momenta of the involved particles are not taken into account.

TABLE I. The selected features of the models used in the current calculations.

Approach	Reaction	Pre/post	E_γ [MeV]	Physics
TCM	γ + nucl.	Pre-post	8–200	Phenomenology
HIPSE	n + nucl.	Pre	20–500	Nuclear
GiBUU	γ + nucl.	Pre	200−10^6	Part. and hadr.
GEMINI++	nucl. (E^*)	Post	8–200	Nuclear
GEM2	nucl. (E^*)	Post	8–2000	Nuclear
EMPIRE	γ + nucl.	Pre-post	8–900	Nucl. and hadr.

One of the most popular is GEMINI++ statistical code [6,21], where the evaporation process is described by the Hauser-Feshbach formalism [22]. The spin, total angular momentum, and orbital angular momentum of the evaporated particle are taken into account in each step. The total energy is conserved. The rotation is treated assuming the rigid body model. The level density parameter formula includes the shell correction to the liquid-drop mass and depends on the excitation energy. The separation energies B_i, nuclear masses, and shell and pairing corrections are taken from Ref. [23].

In the current work the Monte Carlo GEMINI++ calculations assume that the excited nucleus is formed with zero angular momentum, which is a good approximation for the photon-induced reaction. At high energies protons or neutrons may escape in a preequilibrium process which leads to $E_{\rm exc} < E_\gamma$. This strongly limits the excitation energy of the residual nucleus. Only for energy $E_\gamma < 100$ MeV photon is totally absorbed and may lead to total angular momentum of the excited nucleus. It is easy to estimate the total angular momentum of the nucleus as $L_{\rm max} = l_{\rm max}\hbar = E_\gamma R_A \hbar$, where R_A (MeV^{-1}) is the absorbing nucleus radius. So the maximal angular momentum is about 10 $\hbar$. We have made an additional calculation for L=10 $\hbar$ and obtained almost no effect on proton and neutron multiplicity. Even if the initial angular momentum is zero, the angular momentum of nuclei in the evaporation cascade is not zero.

For a short summary, Table I gives the selected features for the approaches used in the current calculation, to underline the differences between them. The GEMINI++ and GEM2 are the deexcitation codes thus as an input need only hot nuclei with a given excitation energy. The main distinction between GiBUU/EMPIRE and HIPSE is the possibility of the description of the γ+nucleus reactions and accounting also hadronic and partonic physics.

III. RESULTS

The GiBUU approach provides cross sections for various reactions. The total cross section is approximately similar to the absorption cross section [24]. Figure 1 shows that for photon energies above 200 MeV, the theoretical (estimated

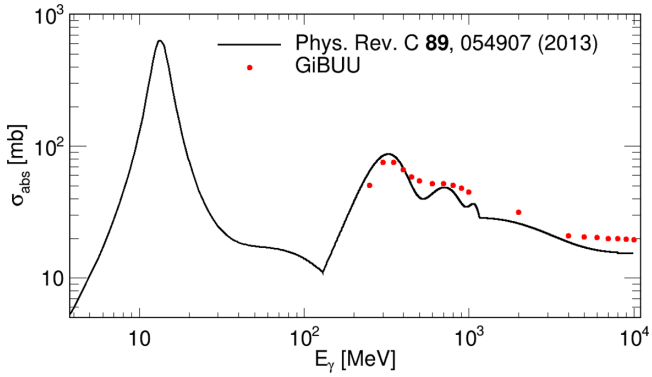


FIG. 1. Photoabsorption cross section for $\gamma + \mathrm{Pb}$ reaction in energy range 10 MeV–100 GeV (full line) compared with the total cross section obtained with the GiBUU model (dots).

by GiBUU) and the experimental photoabsorption cross sections agree.

The collision of the photon and nucleus is very interesting process and many approaches try to describe it. The mechanisms of photon-nucleus interaction are energy dependent. In the UPC, different photon energies and therefore various mechanisms come into play. One has to consider the situation when photons only slightly excite nucleus (giant dipole resonances), photon knock-out of one nucleon, excitation of nucleon resonances (mainly Δ), many exclusive processes on individual nucleons, and, finally, partonic reactions on nucleons (nucleon break-up). Afterwards, in all cases, various particles can be emitted during de-excitation by means of evaporation or by more violent processes.

In most cases of interest of this work, the result of a collision considered has to be a highly excited nuclear system. There are various approaches to estimate its excitation energy. One of them is the energy balance, where part of the photon energy is taken as kinetic energy of evaporated particles and the Q values. This procedure is applied, for example, in the HIPSE model [Fig. 2(a)]. The HIPSE model is usually applied for reactions up to the Fermi energy, thus during the reagregation stage the energy and momentum conservation laws are fulfilled, allowing us to build clusters. In the fragmentation energy regime the internal energy forbids creation of bigger systems. During the thermalization phase, the full internal energy is divided among the formed prefragments, allowing an estimation of their excitation energy.

In the case of approaches used for description of nucleus behavior when the nuclear processes are saturated, it is very difficult to discuss about prefragments. For our purposes, the result of the collision $\gamma + \mathrm{Pb}$ was translated into prefragments assuming that nucleons close to each other in space could form clusters and even heavier nuclei. The energy conservation law is not really the best method to estimate the excitation energy of such a system. Thus, assuming that one missing particles takes away on average 13 MeV the excitation energy left in the compound system is extracted from photon energies. In the GiBUU approach, the sum of energies taken by

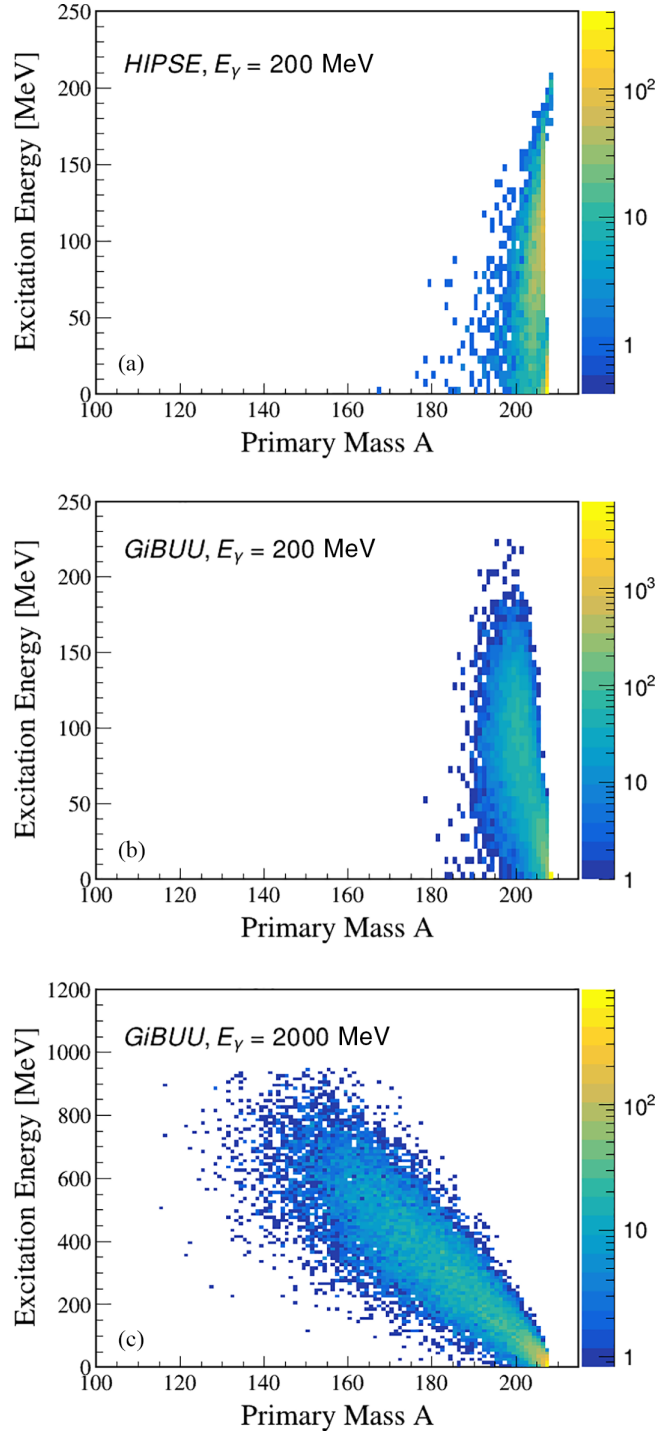


FIG. 2. Distribution of the primary mass and its excitation energy predicted in the naively adopted HIPSE [$E_\gamma = 200$ MeV (top)] and GiBUU [$E_\gamma = 200$ MeV (middle) and $E_\gamma = 2000$ MeV (bottom)].

missing nucleons (vacancies) generate the excitation energy [Figs. 2(b) and 2(c)]. Very high excitation energies could be generated within the GiBUU model. The HIPSE and GiBUU give different excitation energy distributions as it is shown in Figs. 2(a) and 2(b).

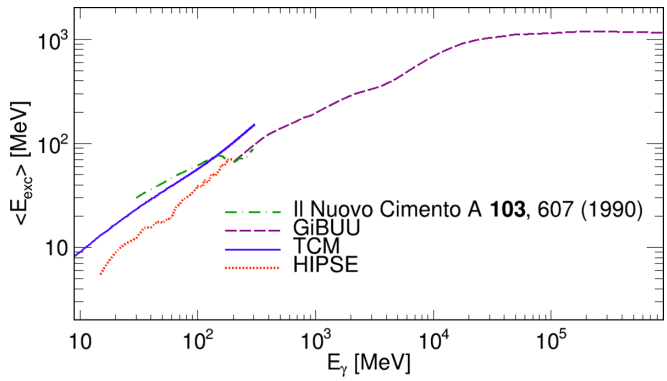


FIG. 3. Average excitation energy as a function of energy of the photon in $\gamma + {}^{208}$Pb collisions in different models.

The comparison of the average excitation energy obtained with various approaches for ^{208}Pb bombarded by photons of various energies are displayed in Fig. 3. The experimental-like data comes from earlier calculation done with an intranuclear cascade model by Guaraldo *et al*. [25] for several preactinides nuclei. The two components model and HIPSE estimation have been already discussed in Ref. [2] but the GiBUU results anticipate the mean excitation energy for the photon-induced reaction also for higher photon energies up to $E_\gamma = 10^6$ MeV. In the low-photon-energy range HIPSE and GiBUU give similar results although the methods of estimation of excitation energy are rather different. It is due to the fact that both models (approximately) conserve the total energy of the system for reactions with $E_\gamma < 200$ MeV.

A. Production of nuclear remnants in $\gamma + {}^{208}$Pb reaction

The nuclei created in this study by GiBUU, are highly excited. The ensemble of nuclei produced after the intranuclear cascade (Fig. 4) depends on the incident photon energy: the higher photon energy, the richer the distribution of masses and charges of the residual nuclei are created. This trend is continued in Fig. 5, where the final mass-charge distribution obtained after remnant deexcitation is displayed.

During the intranuclear cascade and thermalization, except of nucleons, also heavier nuclear objects can be emitted. This is known from studies of nuclear spallation processes [26–29]. Unfortunately, in the GiBUU model, the formation and emission of nuclear clusters is disregarded. Thus, resulting particle multiplicities are, to some extent, biased by this model restriction.

Final distribution of nuclei, when remnant deexctitation is simulated, are shown in Fig. 5. In extreme case, very exotic nuclei can be generated up to the proton or neutron drip lines or even behind. The deexcitation of produced hot nuclei are estimated with GEMINI++ or GEM2. Figure 5 displays the final mass-charge distribution for two photon energies $E_\gamma = 200$ MeV and 2000 MeV. The evaporation residues are above mass 150, the fission fragments are in the mass range (50–150) and intermediate mass fragments are below mass 50. The particle and γ emission are allowed in every step of

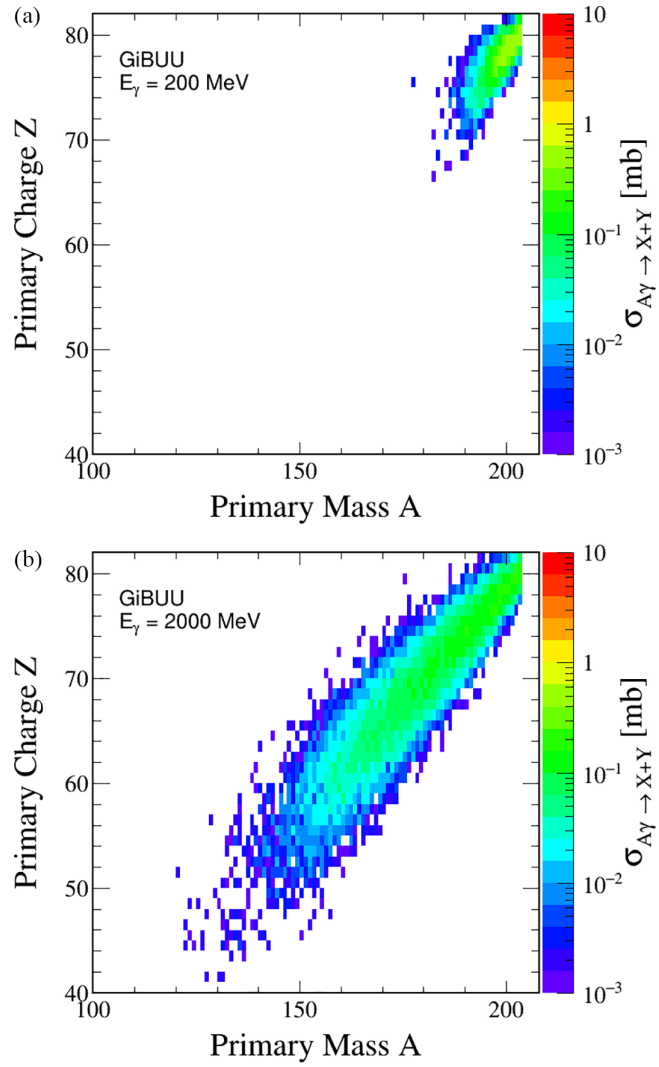


FIG. 4. Cross section for production of primary fragments: GiBUU for collisions of 200-MeV and 2000-MeV photons in $\gamma + {}^{208}$Pb reaction.

deexcitation. Here, apart from protons and neutrons, also α, deuterium, and tritium evaporation is taken into consideration.

B. Proton and neutron multiplicities in the $\gamma + {}^{208}$Pb reaction

The GiBUU approach allows only for emission of nucleons. No α particles or other clusters are included. This limitation results in a possible enhancement of the neutron and proton multiplicities.

Experimental data for the average neutron multiplicities are available only up to $E_\gamma = 140$ MeV [30–32]. Their extrapolation (taken from Ref. [33]) are compared (Fig. 6) with the mean neutron number emitted during the intranuclear cascade phase in GiBUU and the final results (GiBUU + GEMINI++). The multiplicities of the emitted particles depend not only on the energy E_γ of the photon, which excites the collision partner, but also on amount of energy stored in equilibration stage.

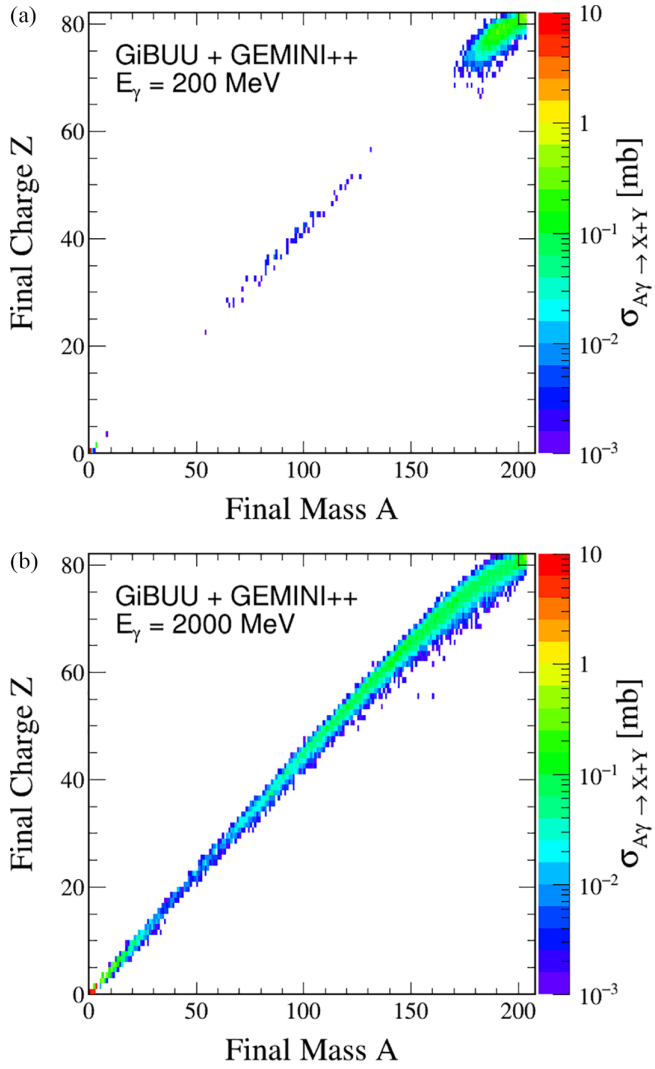


FIG. 5. Cross section for production of final nuclei: GiBUU + GEMINI++ for 200-MeV and 2000-MeV photons in $\gamma + {}^{208}$Pb reactions.

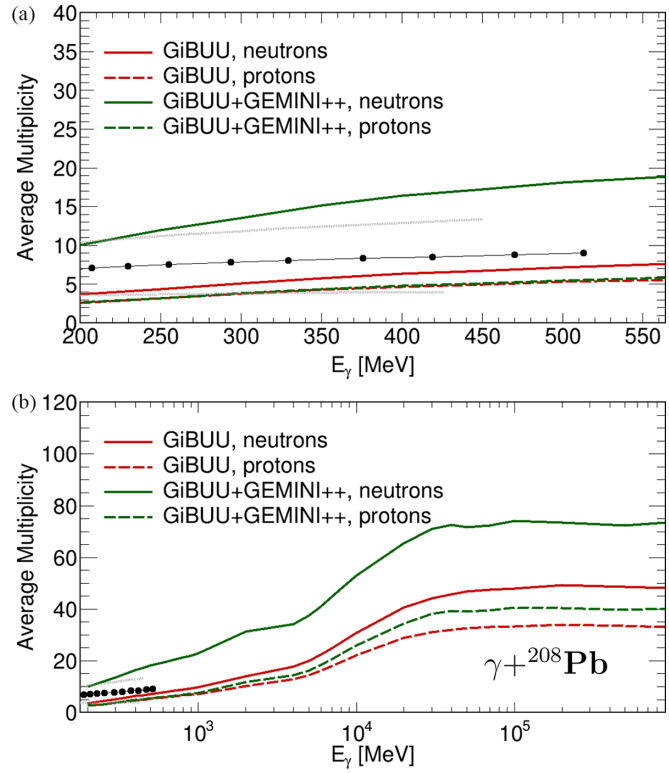


FIG. 6. Average neutron multiplicity: preequilibrium obtained in GiBUU (red line), final results with GEMINI++ deexcitation code (green line); (a) zoomed on the photon energy $E_\gamma = (200,\ 600)$ MeV and (b) for full energy range up to $E_\gamma = 10^6$ MeV. The extrapolation of experimental data [32,33] (black dots) and band of uncertainty (dotted lines) are shown. The full lines are for neutrons and the dashed ones are for protons.

The centroid of the neutron multiplicity distribution is moving towards the higher numbers when the deexcitation stage is included (GiBUU+GEMINI++) in comparison to the primary emission (GiBUU). The total multiplicities of neutrons coming from both stages seem to be too large compared to the experimental data shown in Fig. 6. The experimental average neutron multiplicity were extracted for photon-induced neutron production from Pb in $E_\gamma =$ (10–140) MeV in Ref. [32] and later extrapolated in Ref. [33] to higher photon energies.

The multiplicity distribution of neutrons strongly depends on excitation energy of residual nucleus. Lets consider the average neutron multiplicity for deexcitation process $\langle M_n^{\text{sec.}} \rangle$.

The combined information from Figs. 3 and 6 is presented in Table II, where the photon energy is translated into the excitation energy of the nucleus and the mean neutron multiplicity is estimated.

This average secondary neutron multiplicities $\langle M_n^{\text{sec.}} \rangle$ come only from the final stage of reaction where particles are emitted during deexcitation of the hot nucleus (see Fig. 6). The situation for proton emission is less regular. Let us compare the red and green dashed lines in Fig. 6. At $E_\gamma = 70$ MeV there is almost no emission of protons. For $E_\gamma = 200$ MeV single proton is emitted with probability (number of single protons per event) of around 0.14. At high excitation energy, $E_\gamma = 2000$ MeV, emission of a bigger number of protons is possible.

Figure 7 shows a comparison of multiplicity distributions of protons and neutrons emitted at two different photon energies: $E_\gamma = 200$ (blue) and 2000 (red) MeV. They are calculated with combination of the GiBUU model for first step of reaction (collision phase) and GEM2 model for deexcitation of remnant nuclei. Large multiplicities of neutrons

TABLE II. The average multiplicity for secondary emission of neutrons $\langle M_n^{\text{sec.}} \rangle$ and protons $\langle M_p^{\text{sec.}} \rangle$ for given excitation energy E_{exc}. (see Figs. 3 and 6).

E_{exc} (MeV)	$\langle E_\gamma \rangle$ (MeV)	$\langle M_n^{\text{sec.}} \rangle$	$\langle M_p^{\text{sec.}} \rangle$
50	70	5	0
150	200	13	0.14
500	2000	25	12

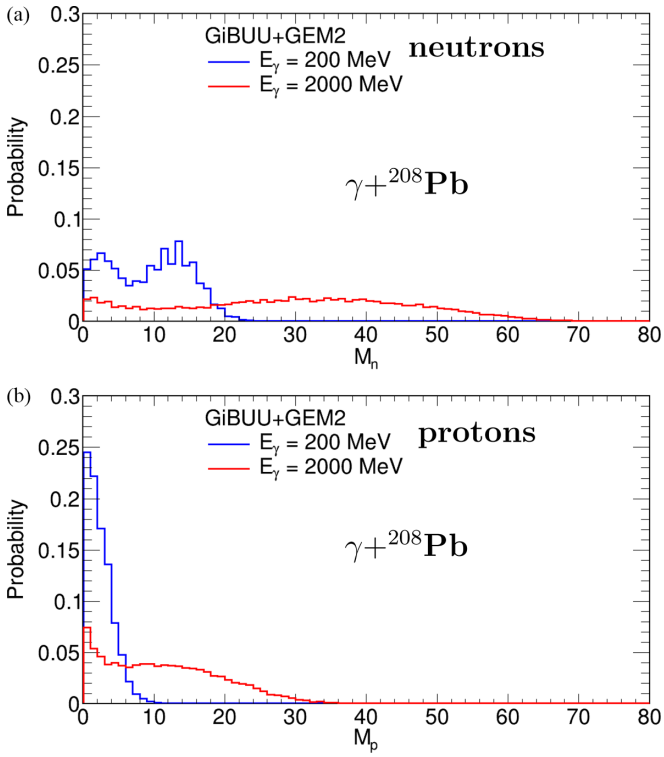


FIG. 7. Neutron (a) and proton (b) multiplicities obtained with GiBUU+GEM2 for deexcitation of the initial nucleus at $E_\gamma = 200$ (blue) and 2000 (red) MeV.

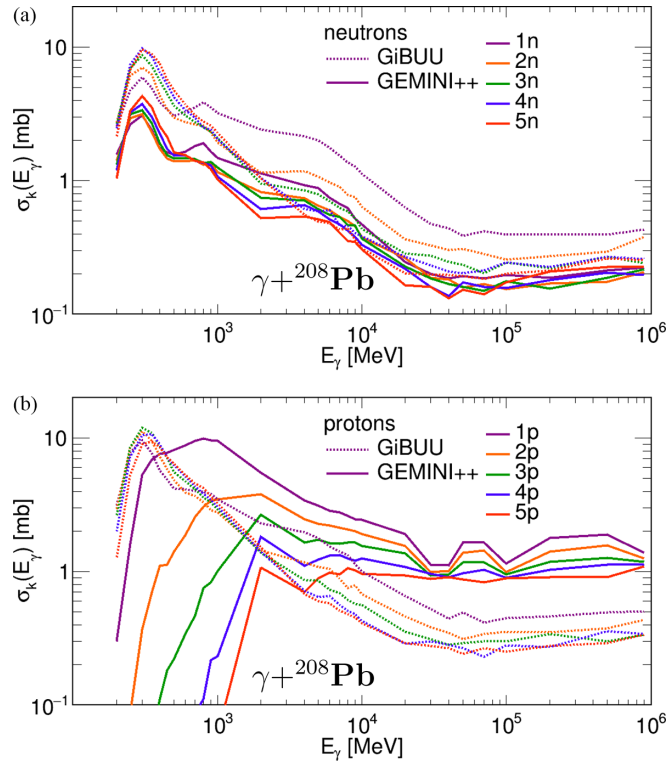


FIG. 8. Neutron (a) and proton (b) cross section for different multiplicities for the emission of given number (k= 1,2,3,4,5) of particles, obtained with GiBUU + GEMINI++.

and protons are obtained, especially at $E_\gamma = 2000$ MeV. For lower photon energies mainly single neutrons and protons are emitted.

Increasing the energy E_γ of photons reacting with ^{208}Pb the distribution of the emitted particles is widening. In the preequilibrium stage calculated with GiBUU starting from 200 MeV, mostly few neutron events are predicted.

Large number of protons that come from the GiBUU, are due to the fact that in preequilibrium stage only nucleons are considered, thus no α, deuterons, tritons, and ^{3}He are taken into account.

The cross section for different multiplicities as a function of photon energy E_γ are presented separately for neutrons [Fig. 8(a)] and protons [Fig. 8(b)].

In the first stage, a few particles are emitted and the primary fragments have enough energy to release secondary particles. Thus, the probability of emission of 1, 2, or 3 neutrons decreases. A similar tendency is visible in Fig. 8(b) for the emission of protons.

Figures 9(a) and 9(b) compare the low multiplicity distributions for nucleons calculated with GiBUU and two different deexcitation codes: GEMINI++ (dashed line) and GEM2 (solid line). The results are very similar, especially for protons. For neutrons the cross sections for photon energy larger than 1 GeV are higher in GEMINI++ than in GEM2.

Although the basic results behind these two models differ, the final results are very similar, especially for protons. For

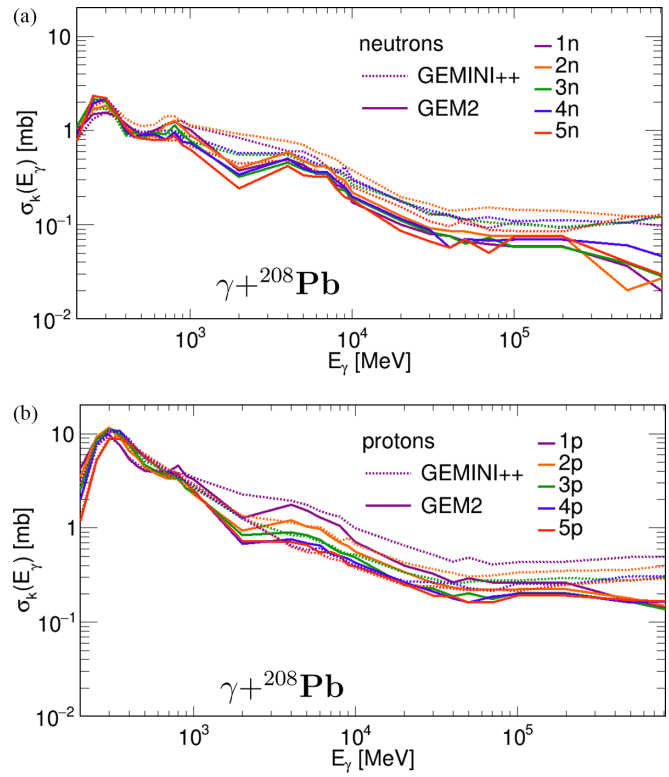


FIG. 9. Comparison of the GEMINI++ (dashed lines) and GEM2 (solid lines) deexcitation models cross section for a given number (k = 1,2,3,4,5) of (a) neutrons and (b) protons.

TABLE III. Different combinations of the models used in the present calculations.

$E_\gamma < 200$ MeV		$E_\gamma > 200$ MeV		
γ+nucleus	Deexcitation	γ+nucleus	Deexcitation	Name
TCM	GEMINI++	TCM	Const. prob.	TCG++
TCM	GEMINI++	GiBUU	GEMINI++	TGG++
TCM	GEMINI++	GiBUU	GEM2	TGG2
HIPSE	GEMINI++	GiBUU	GEMINI++	HGG++

neutrons the cross section for photon energy larger than 1000 MeV are somewhat higher in GEMINI++ than in GEM2.

C. Integrated UPC cross sections

The method, to obtain the cross section for the ultrarelativistic ultraperipheral Pb + Pb reaction at $\sqrt{s_{NN}} = 5.02$ TeV was described in detail in Ref. [2]. The main idea is the integration of the electromagnetic flux with probabilities for a given number of neutrons or protons over a wide photon energy range and the impact parameter. The following combinations of models are used to estimate the neutron or proton emission or remnant production (presented also in Table III):

(1) The two-component model (TCM - Dirac delta + steplike probability function including GEMINI++) combined with GEMINI++ for $E_\gamma < 200$ MeV and constant probability for higher photon energies (TCG++);

(2) The two-component model with GEMINI++ for $E_\gamma <$ 200 MeV and GiBUU with GEMINI++ for higher energies (TGG++);

(3) The two-component model with GEMINI++ for $E_\gamma <$ 200 MeV and GiBUU with GEM2 for higher energies (TGG2);

(4) The HIPSE with GEMINI++ for $E_\gamma < 200$ MeV and GiBUU with GEMINI++ for higher energies (HGG++).

(5) The EMPIRE model that covers the photon energy up to 900 MeV. Constant probability at large energies was introduced already in our previous paper [2]. Of course, this is a strong assumption but was inspired by the Saclay experimental data [32] and used in Refs. [33,34]. Long tails of probability in neutron and proton energies are probably due to preequilibrium processes as the ones considered in GiBUU and also in Sec. IV of the present paper.

In Table IV we compare results obtained with GiBUU combined with two deexcitation models: GEMINI++ and GEM2 and with the TCM approach [Eq. (3)] applied naively to proton emissions.[2] Here, only one photon exchange is taken into consideration (see Fig. 1(a) from Ref. [2]) as the multiple photon exchange were estimated to give contribution of the order of 10%. Similar results were presented in Ref. [35]. In comparison to TCM the calculation with the GiBUU model combined with deexcitation codes gives almost 2 times lower

[2]The model was constructed in Ref. [2] to understand neutron emissions.

TABLE IV. Total cross sections (in barn) for a fixed number of neutron in UPC for reaction of ^{208}Pb + ^{208}Pb with energy $\sqrt{s_{NN}} =$ 5.02 TeV. The integration is done only for energies $E_\gamma > 200$ MeV. The two-component model (TCM) with GEMINI++ and constant neutron probability equal to $P(E_\gamma = 200$ MeV) – (TCG++) are compared to the GiBUU with GEMINI++ (TGG++) and the GiBUU with GEM2 (TGG2) results. Here only one photon exchange is taken into consideration [see Fig. 1(a) from Ref. [2]].

	TCG++	TGG++	TGG2
$1n$	2.294	1.308	1.160
$2n$	3.210	1.553	1.207
$3n$	2.513	1.160	1.155
$4n$	3.324	1.325	1.136
$5n$	2.940	1.156	1.079

cross sections. Both GEMINI++ and GEM2 show a similar tendency as seen already in Fig. 9.

The total cross sections for a neutron, proton emission, and isotope production are compared for various scenarios in Table V. Both TCM and GiBUU combined with GEMINI++ or GEM2 badly fail to describe the large ALICE cross section [8] for the one-proton emission ($\sigma_{1p} \approx 40$ b). While for neutron channels all models give right order of magnitude, the situation for proton channels is very different. Here all models underestimate the new ALICE proton data [8]. The situation with isotope production is similar.

In Fig. 10 presented is a cross section calculated with the combination of GiBUU and GEMINI++ models. As expected and measured in Ref. [8] the dominant yield is foreseen for targetlike nuclei close to $A = 208$ and $Z = 82$. According

TABLE V. Total cross sections (in barns) for a fixed number of neutrons and protons emissions and isotope production in UPC with energy 5.02 TeV. The cross-section integration ingredients depends on the photon energies. For photon energies $E_\gamma < 200$ MeV available are as follows: the TCM, HIPSE, and EMPIRE approaches. For energies $E_\gamma \geqslant 200$ MeV, the constant probability (TCG++) and the GiBUU with GEMINI++ (TGG++) and GEM2 (TGG2); HIPSE with GiBUU and GEMINI++ (HGG++) as well as EMPIRE results are presented. Here, only one photon exchange is taken into consideration [Fig. 1(a) from Ref. [2]].

E_γ	TCG++	TGG++	TGG2	HGG++	EMPIRE	ALICE [1,8]
$1n$	98.79	97.37	97.23	113.21	98.90	108.4 ± 3.90
$2n$	25.31	23.24	22.90	14.34	23.39	25.0 ± 1.30
$3n$	6.03	4.24	4.23	4.24	3.91	7.95 ± 0.25
$4n$	6.32	3.69	3.51	3.41	2.28	5.65 ± 0.33
$5n$	4.91	2.56	2.49	2.79	1.05	4.54 ± 0.44
$1p$	6.59	12.54	13.18	5.25	2.36	40.4 ± 1.6
$2p$	0.44	6.63	3.71	4.74	0.01	16.8 ± 3.7
$3p$	0.01	3.40	2.35	4.60	0.01	6.8 ± 2.2
Pb	150.47	125.12	124.87	130.7	129.51	157.5 ± 4.6
Tl	5.86	5.42	4.97	7.24	0.001	40.4 ± 1.6
Hg	9.67	4.88	4.59	4.92	0.0007	16.8 ± 3.7
Au	2.43	4.29	3.97	4.25	0.00001	6.8 ± 2.2

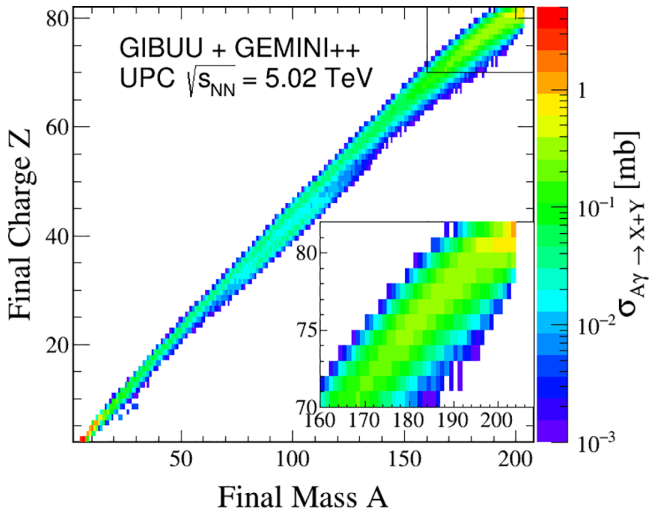


FIG. 10. Cross section for production of nucleus remnants in ^{208}Pb + ^{208}Pb UPC. The inset plot is the zoom on mass range A = (160–208).

to our predictions, except the lead nuclei, in ultraperipheral collisions the final deexcited nuclei of mass $A > 170$ and charge $Z > 70$ are mostly populated.

Comparing Tables IV and V it is clear that most of the contribution from the energy region $E_\gamma < 200$ MeV as there the absorption cross section is large (see Fig. 1).

IV. ON THE PREEQUILIBRIUM PRODUCTION OF ONE PROTON CHANNELS ABOVE GIANT DIPOLE RESONANCE

The $\gamma + {}^{208}$Pb $\to$ hadrons is the main channel of the proton/neutron production in ^{208}Pb + ^{208}Pb UPC collisions. The emission of nucleons in scattering photons off nuclei was studied some time ago for ^{12}C(γ, pn) and ^{12}C(γ, pp) [36] using tagged photons at MAMI with E_γ = 150–700 MeV and more recently in a Ph.D. thesis of R. Williams [37] also for $\gamma + {}^{12}$C collisions at JLab. In the latter case the emphasis was on multiproton production. To our knowledge, no experimental input for our $\gamma + {}^{208}$Pb reaction exists. Therefore, in the following we have to rely on models.

As shown in Table V the cross section for one-proton ($1p$) emission ($1p \equiv 1px$, where x denotes production of anything but not protons) in the statistical codes is very small compared to the huge cross section of about 40 b measured by the ALICE collaboration [8].

At low energies photons interact with the whole nucleus and excite giant dipole resonance (GDR). At higher energies photons start to interact with individual nucleons inside the nucleus. The interaction of photons with nucleons is complicated and strongly energy dependent as different mechanisms play the role for $E_\gamma > 150$ MeV. Only a few simple final states were carefully measured at Bonn Elsa, MAMI at Mainz or at JLab. Some simple final states are included in intranuclear cascade codes such as PICA [35] or RELDIS [34]. We will show below that even this complicated and elaborated treatment may be not sufficient. We wish to note here that even for $\gamma + d \to p + n$ process the mechanism of reaction is not well understood [38].

At even larger photon energies, say, $E_\gamma > 1$ GeV, one is not able to control all final states and one is forced to concentrate rather on inclusive production of protons and neutrons. This high-energy region of the γN interaction and its impact on the γA interaction was not well documented in the literature.

In this section we discuss how the physics of γA interactions changes when increasing gradually photon energy. Intentionally, restricted by available data, we will focus on production of one-proton and one-neutron only in processes initiated by collisions of photon with individual nucleons. The large cross section for one-proton emission measured recently by the ALICE collaboration is particularly interesting as no existing model can explain it.

In this section we will try to estimate the maximally available cross section for the one-proton emission.

Our total photoabsorption cross section is a sum of four different components [39]:

(i) giant dipole resonance, $\sigma_{\gamma A}^{\rm GDR}(\omega)$,
(ii) quasideuteron mechanism, $\sigma_{\gamma A}^{\rm QD}(\omega)$,
(iii) nucleon resonance region,[3] $\sigma_{\gamma A}^{\rm res}(\omega)$,
(iv) partonic region, $\sigma_{\gamma A}^{\rm part}(\omega)$

$$\sigma_{\gamma A}(\omega) = \sigma_{\gamma A}^{\rm GDR}(\omega) + \sigma_{\gamma A}^{\rm QD}(\omega) + \sigma_{\gamma A}^{\rm res}(\omega) + \sigma_{\gamma A}^{\rm part}(\omega), \quad (6)$$

where ω is photon energy. As will be discussed in the following, for lowest photon energies (GDR), practically no protons are emitted. At higher photon energies, photon interacts rather with individual nucleons and not with the whole nucleus. While the produced neutron can be easily emitted, the proton experiences a Coulomb barrier. The Woods-Saxon single-particle potential for neutrons and protons (including Coulomb part) are illustrated in Fig. 11 as a function of distance from the center-of-mass of ^{208}Pb nucleus. The parameters of the potentials were tested in several papers [40–44]. Proton emission becomes easier when $E_p > E_{\rm barrier} \approx 10$ MeV, which seems to have smaller influence for $E_\gamma > 200$ MeV.

It is obvious that the cross section for $1p$ emission must be smaller than the photoabsorption cross section for any ω. Then the absolutely maximal estimation of the one-proton cross section in UPC can be approximated as:

$$\max\{\sigma_{AA\to 1p}\} = \max\left\{\sigma_{AA\to p}^{\rm QD}\right\} + \max\left\{\sigma_{AA\to p}^{\rm res}\right\} + \max\left\{\sigma_{AA\to p}^{\rm part}\right\}, \quad (7)$$

where cross sections for one-side $1p$ emission (forward or backward) in UPC can be obtained as

$$\max\left\{\sigma_{AA\to 1p}^{\rm QD}\right\} \approx \int N(\omega, b)\sigma_{\gamma A}^{\rm QD}(\omega)\, d^2b d\omega,$$

$$\max\left\{\sigma_{AA\to 1p}^{\rm res}\right\} \approx \int N(\omega, b)\sigma_{\gamma A}^{\rm res}(\omega)\, d^2b d\omega,$$

[3]The "resonance" region includes also nonresonance contributions.

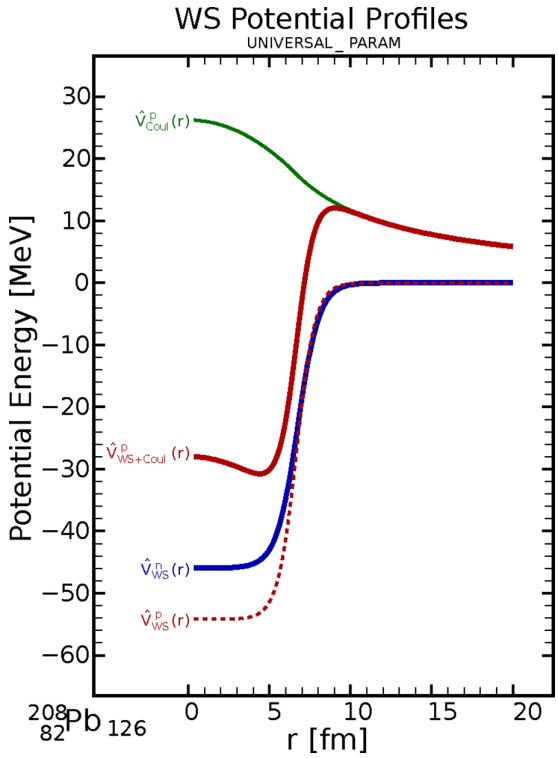


FIG. 11. The Woods-Saxon single-particle potential for neutrons (blue line) $\hat{V}^n_{\rm WS}$ and protons (dashed red line) $\hat{V}^p_{\rm WS}$, Coulomb part $\hat{V}^p_{\rm WS+Coul}$ (green line) and their sum (solid red lines) as a function of distance from center-of-mass of ^{208}Pb nucleus.

$$\max\left\{\sigma^{\rm part}_{AA\to 1p}\right\} \approx \int N(\omega,b)\sigma^{\rm part}_{\gamma A}(\omega)\, d^2b d\omega. \tag{8}$$

Similar equation can be written for one-neutron preequilibrium emissions. If we apply parametrizations of different γPb photoabsorption components in (7) used in Ref. [39] we get:

$$\begin{aligned}\max\left\{\sigma^{\rm QD}_{AA\to p}\right\} &= 12.62\ b,\\ \max\left\{\sigma^{\rm res}_{AA\to p}\right\} &= 39.31\ b,\\ \max\left\{\sigma^{\rm part}_{AA\to p}\right\} &= 34.29\ b.\end{aligned} \tag{9}$$

Adding maximal values for each component we get $\max(\sigma_{AA\to 1p}) = 85$ b which is only about two times bigger than the cross section measured by the ALICE collaboration.

The estimation above is an absolute upper limit. Not only protons but also neutrons can be produced in $\gamma + N$ collisions. The cross section with proton or neutron emission should not exceed the photoabsorption cross section. This must be so for each component (i), included in modeling the absorption cross section. Then for different reaction mechanisms (i) the following simple sum rule must be fulfilled:

$$\begin{aligned}\sigma^{(i)}_{\gamma A}(\omega) > Z\left(\sigma^{(i)}_{\gamma p\to pX}(\omega)+\sigma^{(i)}_{\gamma p\to nX}(\omega)\right)\\ +N\left(\sigma^{(i)}_{\gamma n\to nX}(\omega)+\sigma^{(i)}_{\gamma n\to pX}(\omega)\right),\end{aligned} \tag{10}$$

where i numerates individual processes. Since for the different distinct mechanisms the relative production of protons and neutrons is approximately known one can set upper limit on

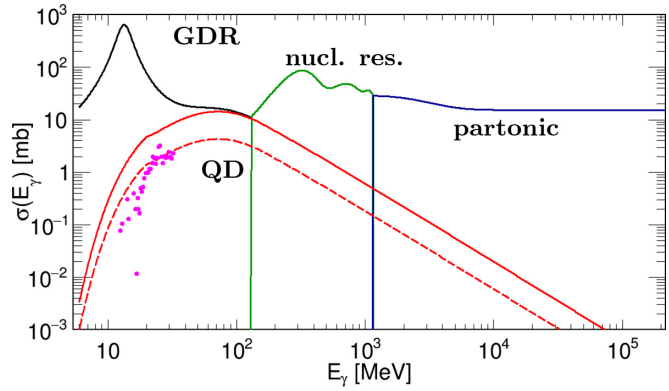


FIG. 12. Cross section for $\gamma + {}^{208}$Pb $\to p$ and our simple fit result. The giant dipole resonance, quasideuteron, nucleon resonances, and partonic components [Eq. (6)] are shown. The experimental points [45] are marked by solid circles. The red dashed line is reduced cross section (see text) in comparison to the red solid line.

$\sigma^{(i)}_{AA\to p}$. This estimation includes production of nucleon resonances and their decay.

The maximal value of the cross section can be therefore lowered. This requires more detailed analyses. We shall discuss all three contributions one by one.

We start from quasideuteron contributions. We assume the simplest form:

$$\sigma^{\rm QD}_{\gamma A\to 1p}(\omega) = C_p \times \sigma^{\rm QD}_{\gamma A}(\omega) \tag{11}$$

and fit C_p to the existing data [45] (see Fig. 12). The giant dipole resonance, quasideuteron, nucleon resonances, and partonic components are shown in Fig. 12. The solid red line corresponds to the QD absorption cross section. However, the proton emission cross section may be smaller than QD component of photoabsorption cross section due to the Coulomb barrier. We rescale the QD absorption cross section to the measured proton emission data. We find $C_p \approx 0.3$. Then $\sigma^{\rm QD}_{AA\to 1p} \approx 3.5$ b, much less than the ALICE result.

Therefore, we also consider the resonance region. A representative example of the reaction to be considered are as follows:

$$\begin{aligned}&\gamma + p \to \Delta^+ \to p\pi^0,\ P = \left|\left\langle\frac{3}{2},\frac{1}{2}\middle|\frac{1}{2},\frac{1}{2},1,0\right\rangle\right|^2 = \frac{2}{3},\\ &\gamma + p \to \Delta^+ \to n\pi^+,\ P = \left|\left\langle\frac{3}{2},\frac{1}{2}\middle|\frac{1}{2},-\frac{1}{2},1,1\right\rangle\right|^2 = \frac{1}{3},\\ &\gamma + n \to \Delta^0 \to n\pi^0,\ P = \left|\left\langle\frac{3}{2},-\frac{1}{2}\middle|\frac{1}{2},-\frac{1}{2},1,0\right\rangle\right|^2 = \frac{2}{3},\\ &\gamma + n \to \Delta^0 \to p\pi^-,\ P = \left|\left\langle\frac{3}{2},-\frac{1}{2}\middle|\frac{1}{2},\frac{1}{2},1,-1\right\rangle\right|^2 = \frac{1}{3}.\end{aligned} \tag{12}$$

Different Δ isobars have different branching fractions. P in Eq. (12) is probability of decay of Δ isobar to one of the πN channels. The relative probability is calculated in terms of the Clebsch-Gordan coefficients. There are other nucleon resonances (not visible in γA collisions) and a few continuum

TABLE VI. Maximal contributions (in barns) of preequilibrium emission of p and n separately for different mechanisms.

σ [b]	Quasi deuteron	Nucl. reson.	High energy	Sum	ALICE [1,8]
$1p$	3.79	18.27	15.56	37.62	40.0 ± 1.6
$1n$	3.79–12.62	21.04	18.73	43.56–52.39	108.4 ± 3.90

contributions like:

$$\begin{aligned} \gamma + p &\to \pi^0 + p, \\ \gamma + p &\to \pi^+ + n, \\ \gamma + n &\to \pi^0 + n, \\ \gamma + n &\to \pi^- + p, \end{aligned} \tag{13}$$

which start at $\omega > 180$ MeV. The $\gamma N \to \pi N$ reactions can be treated microscopically including meson-exchange currents and channel coupling [46]. This treatment starts to be almost impossible already for $\gamma N \to \pi\pi N$ reactions. Therefore microscopic treatment is limited only to some energy windows.

Another strongly populated final state is exclusive vector meson production V:

$$\begin{aligned} \gamma + p &\to V + p, \\ \gamma + n &\to V + n, \end{aligned} \tag{14}$$

where $V = \rho^0, \omega, \phi, J/\psi$.[4] The $\gamma N \to VN$ reactions can be successfully calculated either within Regge approach [47] (see also Ref. [48] within tensor-pomeron model) or dipole model approach [49]. However, the $\gamma N \to VN^*$ processes were not carefully studied within microscopic models, but they also lead to sizable production of protons or neutrons.

The cross section for $\gamma + p \to \rho^0 + p$ only weakly depends on energy and is 10–20 μb (see, e.g., Ref. [48]). At sufficiently high energy the cross section for $\gamma A \to \rho^0$ can be roughly estimated as $A\sigma(\gamma p \to \rho^0 p)$. Then the corresponding contribution to $\gamma + A \to p$ is therefore about 0.8–1.6 mb, which constitutes sizable fraction of the $\gamma + A$ absorptive cross section (see Fig. 6). This inelastic cross section is of the same order of magnitude as $\gamma + A \to \rho^0 + A$ [50].

More processes were discussed, e.g., in Refs. [34,35]. Our estimation here has advantage that it exhausts by construction the absorption cross section for processes on individual nucleons. For the sake of simplicity, assuming that the Δ resonances are representative for the whole "resonance" region, we write

$$\begin{aligned} \sigma^{\rm res}_{AA\to 1p} &\approx \left(\frac{2}{3}\frac{Z}{A} + \frac{1}{3}\frac{N}{A}\right)\sigma^{\rm res}_{AA}, \\ \sigma^{\rm res}_{AA\to 1n} &\approx \left(\frac{1}{3}\frac{Z}{A} + \frac{2}{3}\frac{N}{A}\right)\sigma^{\rm res}_{AA}. \end{aligned} \tag{15}$$

We can see that even including the quasideuteron and resonance regions we are not able to understand the ALICE result for one proton emission (Table VI).

Therefore we consider also the highest energy, "partonic," component. The production of protons or neutrons is subjected to the mechanism of nucleon remnant fragmentation (see, e.g., Ref. [51]). The HERA data on leading neutron and proton production in $\gamma^* p$ collisions showed that we did not fully understand the underlying physics before the HERA results. New mechanisms were proposed in Refs. [52] and [53]. Combining the conventional at that time and "new" mechanisms requires a hybrid approach for fixed target experiments (see, e.g., Ref. [54]). Since in the current paper we are interested just in proton and neutron production, we should used here such a hybrid model.

We have to consider first elementary γp or γn cross sections. The high-energy component cross section (Table VI) on proton can be decomposed into a sum of three terms, named for brevity diffractive, Sullivan and hadronization:

$$\begin{aligned} \sigma_{\gamma p\to p} &= \sigma^{\rm diff}_{\gamma p\to p} + \sigma^{\rm Sull}_{\gamma p\to p} + \sigma^{\rm hadr}_{\gamma p\to p}, \\ \sigma_{\gamma p\to n} &= \sigma^{\rm diff}_{\gamma p\to n} + \sigma^{\rm Sull}_{\gamma p\to n} + \sigma^{\rm hadr}_{\gamma p\to n}. \end{aligned} \tag{16}$$

In an analogous way for production for scattering on neutron:

$$\begin{aligned} \sigma_{\gamma n\to p} &= \sigma^{\rm diff}_{\gamma n\to p} + \sigma^{\rm Sull}_{\gamma n\to p} + \sigma^{\rm hadr}_{\gamma n\to p}, \\ \sigma_{\gamma n\to n} &= \sigma^{\rm diff}_{\gamma n\to n} + \sigma^{\rm Sull}_{\gamma n\to n} + \sigma^{\rm hadr}_{\gamma n\to n}. \end{aligned} \tag{17}$$

The decomposition in Eq. (16) and Eq. (17) is written in the works of one of the coauthors of the present paper [54–57]. The diffractive components can be estimated as:

$$\begin{aligned} \sigma^{\rm diff}_{\gamma p\to p} &\approx 0.1\ \sigma_{\gamma p\to p}, \\ \sigma^{\rm diff}_{\gamma n\to n} &\approx 0.1\ \sigma_{\gamma n\to n}. \end{aligned} \tag{18}$$

The value 0.1 is approximate contribution of diffractive processes $\gamma + p \to p + X$, i.e., processes with exchange of the pomeron. In this case the outgoing proton (or neutron) cannot receive a large kick of energy or momentum.

This means:

$$\begin{aligned} \sigma^{\rm diff}_{AA\to p} &\approx 0.1\frac{Z}{A}\sigma^{\rm part}_{AA}, \\ \sigma^{\rm diff}_{AA\to n} &\approx 0.1\frac{N}{A}\sigma^{\rm part}_{AA}. \end{aligned} \tag{19}$$

We consider diffractive processes on protons (with fraction $\frac{Z}{A}$ in the target nucleus) or on neutrons (with fraction $\frac{N}{A}$ in the target nucleus). Then the remaining diffractive components for $p \to n$ and $n \to p$ are small and can be ignored in our simple estimation. For the so-called Sullivan processes[5] one has

$$\begin{aligned} \sigma^{\rm Sull}_{\gamma p\to p} &= \sigma^{\rm Sull}_{\gamma n\to n} = 0.35\ \tfrac{1}{3}\sigma_{\gamma p\to p}, \\ \sigma^{\rm Sull}_{\gamma p\to n} &= \sigma^{\rm Sull}_{\gamma n\to p} = 0.35\ \tfrac{2}{3}\sigma_{\gamma p\to p}. \end{aligned} \tag{20}$$

[4]The p/n proportions there are different than for Δ resonances discussed above.

[5]The Sullivan processes are the only known to us explanation of the Gottfried sum rule violation for deep inelastic scattering [55,56].

The 0.35 is an approximate probability to find (virtual) pion in the nucleon. Then reaction on quarks in the pion is called Sullivan process. The virtual pions in the nucleon allow to explain the Gotfried sum rule violation: $\int dx \frac{1}{x}[F_2^{ep}(x) - F_2^{en}(x)] \neq \frac{1}{3}$ [55,56]. The $\frac{2}{3}$ is a relative probability to find charged pion and $\frac{1}{3}$ is a relative probability to register neutral pion. These two numbers reflect isospin structure of the couplings of pions to nucleons (see, e.g., Ref. [58]).

Combining the results for UPC,

$$\sigma_{AA\to p}^{\text{Sull}} \approx \left(\frac{Z}{A}0.35\frac{2}{3} + \frac{N}{A}0.35\frac{1}{3}\right)\sigma_{AA}^{\text{part}},$$
$$\sigma_{AA\to n}^{\text{Sull}} \approx \left(\frac{Z}{A}0.35\frac{1}{3} + \frac{N}{A}0.35\frac{2}{3}\right)\sigma_{AA}^{\text{part}}. \quad (21)$$

Assuming only light u and d quarks and antiquarks in p and n and $u(x) \propto d(x)$ [SU(2) symmetry of quark distributions] we get

$$\sigma_{\gamma n}^{\text{hadr}} = \frac{2}{3}\sigma_{\gamma p}^{\text{hadr}},$$
$$\sigma_{\gamma n}^{\text{hadr}} = \sigma_{\gamma p}^{\text{hadr}} \quad (22)$$

for valence and sea dominance, respectively. The contributions with $1p$ or $1n$ from that component is estimated as

$$\sigma_{\gamma p\to p}^{\text{hadr}} = 0.7\ \sigma_{\gamma p}^{\text{hadr}},$$
$$\sigma_{\gamma p\to n}^{\text{hadr}} = 0.3\ \sigma_{\gamma p}^{\text{hadr}},$$
$$\sigma_{\gamma n\to n}^{\text{hadr}} = 0.7\ \sigma_{\gamma n}^{\text{hadr}},$$
$$\sigma_{\gamma n\to p}^{\text{hadr}} = 0.3\ \sigma_{\gamma n}^{\text{hadr}}. \quad (23)$$

These are typical numbers in hadronization models (see, e.g., Ref. [51]). The hadronization component can be found by solving the set of Eq. (22) and

$$Z\cdot\sigma_{\gamma p}^{\text{hadr}} + N\cdot\sigma_{\gamma n}^{\text{hadr}} \approx \sigma_{\gamma A}^{\text{hadr}}, \quad (24)$$

where the hadronization component can be approximated as

$$\sigma_{\gamma A}^{\text{hadr}} \approx 0.55\ \sigma_{\gamma A}^{\text{part}}. \quad (25)$$

A typical probability of partonic effects in the hybrid models at high (virtual) photon energies is 0.55.

No shadowing effects are included above. It would reduce somewhat our estimate.

Finally, we get for the hadronization component:

$$\sigma_{AA\to p}^{\text{hadr}} = \left(\frac{Z}{A}0.7\cdot 0.55 + \frac{N}{A}0.3\cdot 0.55\right)\sigma_{AA}^{\text{part}},$$
$$\sigma_{AA\to n}^{\text{hadr}} = \left(\frac{Z}{A}0.3\cdot 0.55 + \frac{N}{A}0.7\cdot 0.55\right)\sigma_{AA}^{\text{part}}. \quad (26)$$

The probability of baryon production in γp or γn collisions is 1, due to baryon number conservation. Mostly protons and neutrons are produced. In our approach we assume that $p \to p$ and $p \to n$ transitions happen in 100% and similarly for $n \to n$ and $n \to p$ transitions. At high energies one may expect a small energy-dependent reduction (less than 5%) due to hyperon production, which we neglect in the current estimation.

Finally, combining the different components, we get the following estimate:

$$\sigma_{AA\to 1p} = 38\ b,$$
$$\sigma_{AA\to 1n} = 44\ b. \quad (27)$$

In Table VI, we show a decomposition of the cross sections (in barns) into components from different regions/mechanisms. While the emission of proton from the quasideuteron was fitted to the data (see Fig. 12), it is rather difficult to make a similar limitation for neutron emission from a quasideuteron. Instead, we show a minimal and maximal value of the cross section. The minimal value was assumed to be that found for proton emission. The cross section for neutron emission should be larger as there is no Coulomb barrier.

One can see that the biggest contributions come from the resonance and partonic regions. Not all models on the market include the partonic contributions. We note that it is impossible to describe the ALICE data for proton production without this high-energy component.

While for the one-proton emission the maximal cross section is compatible with the ALICE data [8], the situation for neutron emission is very different. It seems, the preequilibrium is a dominating mechanism of one-proton emission, in contrast the neutrons have very large equilibrium component (see Ref. [2]). Therefore the cross section for neutron emission above should not be compared with the ALICE neutron data [1]. It represents rather microscopic explanation of long-energy tails in probability functions used in the TCM.

Please note that in the estimation in this section we have completely neglected final-state interactions (FSI) of produced and outgoing proton and neutron in the cold nuclear medium. The rough agreement of our estimate with the ALICE data may mean that potentially complicated nuclear effects in the intranuclear cascade almost do not change the rate of $1p$ emissions. The proton FSI is expected to reduce the population of one-proton channel. On the other hand neutron FSI could enhance the population of one-proton channel. The two effects work in opposite directions and tend to compensate each other. However, precise estimation of this effect is not easy.

The protons (and neutrons) formed in diffractive processes may have too small energies to escape from nuclei, and therefore our estimate of $\sigma_{AA\to 1p}$ stays an upper limit for the single-proton emissions.

The preequilibrium emission of one-proton with energy-dependent probability,

$$P_p(\omega) \approx \sigma_{AA\to 1p}(\omega)/\sigma_{AA\to X}(\omega), \quad (28)$$

starts a statistical cascade based on excited $^{207}\text{Tl}^*(E_{\text{exc}})$ while single-neutron emission initiates the cascade based on excited $^{207}\text{Pb}^*(E_{\text{exc}})$. The energy-dependent probabilities $P_p(\omega)$ and $P_n(\omega)$ could be extracted from Fig. 9. The chains mentioned above are initiated with probabilities $P_{^{207}\text{Tl}}(\omega) = P_{1p}(\omega)$ and $P_{^{207}\text{Pb}}(\omega) = P_{1n}(\omega)$, which is about $\frac{1}{2}$. We estimate that for $\omega > 200$ MeV the excitation energy of the initial ^{207}Tl or ^{207}Pb is typically of the order of $E_{\text{exc}} \in (0, 30\ \text{MeV})$, which is relatively low.

However, it is rather difficult to calculate the initial distribution of excitation energies $E_{\rm exc}$ in ^{207}Tl or ^{207}Pb, respectively.

The current estimation of preequilibrium effects has also interesting consequences for neutron emission. If there were only preequilibrium emissions of neutrons the $\frac{d\sigma}{dE_n}$ distribution in the fixed target case (E_n is energy in the target rest frame) would be approximately Gaussian [39]. The preequilibrium emission of neutrons causes appearance of high-energy tails in the $\frac{d\sigma}{dE_n}$ distribution observed in Ref. [30] for fixed-target experiment $\gamma + \mathrm{Pb}$. Our estimate for one-neutron emission is that about 40% of $1n$ emissions (40–45 b of the preequilibrium component compared to 100–110 b measured by the ALICE Collaboration [1]) are in the tail. This seems to be roughly consistent with the observation in Ref. [31]. Summarizing, the preequilibrium effects discussed here are responsible for neutron high-energy tail observed long time ago at Frascati and Saclay.

A. Comment on *NN* rescattering in the intranuclear cascade and short-range *pn* correlations

In the last section, we discussed preequilibrium production of protons and neutrons neglecting FSI effects. The FSI may lead to elastic and inelastic collisions in the nuclear matter. The nucleon hit by the photon is scattered and may interact with other nucleons in the target which will be rescattered. There are the following combinations of such interactions possible:

(1) p(primary) + p(rescat.) $\rightarrow 2p$,
(2) p (primary) + n (rescat.) $\rightarrow pn$,
(3) n (primary) + p (rescat.) $\rightarrow pn$,
(4) n (primary) + n (rescat.) $\rightarrow 2n$,

provided kinetic energies of nucleons are bigger than Fermi energy due to Pauli exclusion principle. By primary we mean here proton or neutron from $\gamma + N$ collision and by rescat. proton or neutron in the nucleus which take part in the rescattering process. It was found in the last decade that the production of pn pair is larger than pp pairs [59–61]. Thus, at low energies, the production of pn pairs is more probable than the two others due to isospin structure of NN interaction. This was not fully explained by theoretical works up to now. Reaction (1) increases number of protons to two, so do not participate to $1p$ channel but may be crucial for $2p$ channel. Reaction (3) creates extra protons to $1p$ channel.

The NN interaction is strongly energy dependent. What are energies of hit nucleons? Everything depends on the mechanism considered:

(A) Quasideuteron: low-energy p or n,
(B) Resonance region: intermediate-energy p or n,
(C) Partonic region: low (diffraction), intermediate (Sullivan), and high (nucleon fragmentation) energy of p or n.

Reaction (A) may be also related to strong pn short-range correlations discussed recently (see, e.g., Ref. [59]). The region (B) was studied in HADES and COSY experiments. The high-energy region was not studied experimentally so far.

The consideration here shows that we can expect enhanced production of pn channel due to FSI and pn short-range correlations (SRC).

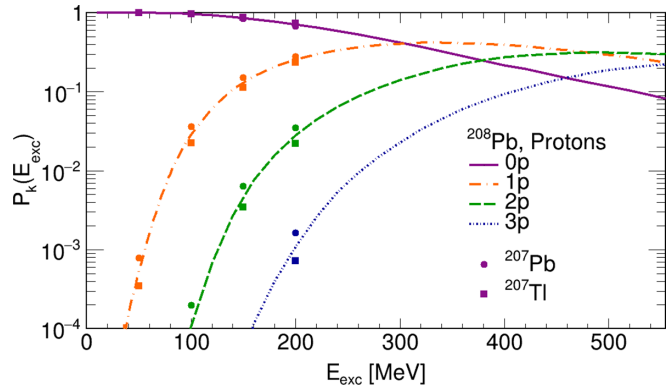


FIG. 13. Probability of emission of $1p$, $2p$, $3p$ as a function of excitation energy calculated within GEMINI++ approach for ^{208}Pb (lines). The circles are for initial ^{207}Pb and squares for initial ^{207}Tl.

The ALICE collaboration measured also pn channel [simultaneous use of proton and neutron ZDCs with the cross section 1.5 b [8], much lower than the cross section for inclusive single-proton production. This sets the upper limit on FSI production of protons in neutron rescattering in $n + p \rightarrow n + p < 1.5$ b. The maximal cross section for pn short-range correlations (SRC) and/or FSI neutron effect would be relatively low compared to our estimate in the previous section. The estimated maximal effect of SRC one could think is 20%[6] of 43 b of our plane-wave impulse approximation (PWIA) prediction for single-neutron production. This estimate of SRC contribution ($\approx$8 b) is much larger than the one measured by the ALICE collaboration. Neutrons may be also produced in the equilibrium statistical emissions. A measurement of $(1p0n)$ channel would be useful to shed more light on the reaction mechanism. The data will be available now in Run3 with triggerless data taking mode.

B. Emission of protons from the equilibrium phase

Let us discuss now the emission of 1, 2, and 3 protons from the equilibrium phase. It is rather difficult to calculate the excitation energy of the residual nucleus. In Fig. 13 we show probability of emission of 1, 2, and 3 protons from the excited nucleus as a function of excitation energy, i.e., energy after the preequilibrium emission of neutron or proton. Here for simplicity, we assume that the initial nucleus is ^{208}Pb.

If the excitation energy of the nucleus is less than 100 MeV, then almost no protons are emitted. For energies greater than 200 MeV, the emission of $1p$, $2p$ becomes sizable. As discussed in previous section the emission of single proton is dominantly due to preequilibrium emission. However, it is very difficult to answer the question whether the emission of $2p$ or $3p$ can be due to equilibrium emissions or due to preequilibrium emission (FSI) discussed in the previous section.

For $E_{\rm exc} = 50$, 100, 150, and 200 MeV we show similar results starting from ^{207}Pb (circles) or ^{207}Tl (squares). There is

[6]This is a rate of SRC correlated NN pairs [60] with assumed dominance of pn correlations confirmed in Ref. [61].

only a small difference compared to the calculation for ^{208}Pb. Our estimate suggests that typically 1 or 2 protons are emitted in the preequilibrium phase (Fig. 6). When at higher photon energies nucleons are emitted in a preequilibrium process, this means that only a part of the initial photon energy is left in the nucleus. Then, residual nuclei are excited to rather small, typically $E_{\rm exc} < 100$ MeV.

V. CONCLUSION

In the present paper, we have discussed the production of protons, neutrons, and nuclear isotopes in ultraperipheral collisions of ^{208}Pb + ^{208}Pb.

Different combinations of preequilibrium and evaporation models have been used. It has been very difficult to reproduce large cross section for one-photon production ($\sigma_{1p} \approx 40$ b), as measured recently by the ALICE collaboration.

The only explanation is that the production of one proton happens in a very broad range of photon energies in all possible photoproduction mechanisms such as emission of protons from interactions on quasideuterons, resonances excited on protons or neutrons or produced in scattering of photons on partons in individual nucleons.

The cross section for single-proton emissions measured by the ALICE collaboration is close to our estimate of the maximum possible cross section from all above mechanisms, as discussed in a separate section. The GiBUU code, when combined with deexcitation models (GEMINI ++ or GEM2), leads to a large cross section for multipole protons production and a small cross section for $1p$ detection which is not supported by the ALICE data.

We have also discussed the difference in cross sections for production of $1p$, $2p$, $3p$, and so on, and that for production of Pb, Tl, Hg, Au, and so on, isotopes. The equality of the corresponding cross sections ($\sigma_{1p} = \sigma_{\rm Tl}$, $\sigma_{2p} = \sigma_{\rm Hg}$, $\sigma_{3p} = \sigma_{\rm Au}$, etc.) is assumed by the ALICE collaboration. However, it is different in models with sizable emission of other charged particles such as d, t, ^{3}He, or α particles such as HIPSE or EMPIRE. For example, a strong α-particle emission would invalidate these equalities. It is rather difficult to test these models with present experimental infrastructure at the LHC where only neutrons or protons can be measured.

No existing models, including TCM, EMPIRE, and GIBUU, can explain huge cross section for $1p$ emission as measured with the help of the proton zero-degree calorimeter. We have presented a careful estimation of maximal possible cross section for $1p$ emission and found that the corresponding ALICE data are very close to this estimate. The new ALICE data for proton production in UPC strongly suggests that single-proton ejection is caused dominantly by preequilibrium processes initiated by photons interacting with individual nucleons in "colliding" nuclei.

The emission of protons in $\gamma + ^{208}$Pb collisions was not well explored so far, especially at higher energies. One possible place to perform such studies, at relatively high photon energies, is JLab. Another option in more distant future is EIC for $e + ^{208}$Pb collisions (virtual photons). It would be be good to plan such experiment(s) already now in order to prepare underlying infrastructure.

ACKNOWLEDGMENTS

We are indebted to Chiara Oppedisano for exchange of information on details of the ALICE ZDC measurements, Or Hen for a discussion about possibility to measure $\gamma + ^{208}$Pb $\to p$ process at JLab, Jan Ryckebusch for exchange of general information about $\gamma + A$ processes, Irene Dedes for preparation of Fig. 11 for displaying neutron and proton single-particle potentials for ^{208}Pb, Mariola Kłusek-Gawenda for discussing several aspects of UPC, and Michał Ciemała for finding us a unique reference for the ^{208}Pb(γ, p) reaction and technical help with GEMINI++ calculations.

DATA AVAILABILITY

The data that support the findings of this article are not publicly available. The data are available from the authors upon reasonable request.

[1] S. Acharya, *et al.*, Phys. Rev. C **107**, 064902 (2023).
[2] P. Jucha, M. Kłusek-Gawenda, A. Szczurek, M. Ciemała, and K. Mazurek, Phys. Rev. C **111**, 034901 (2025).
[3] P. Jucha, K. Mazurek, M. Kłusek-Gawenda, M. Ciemała, A. Szczurek, Y. Shevchuk, and S. Słotwinski, Acta Phys. Pol. B Proc. Suppl. **18**, 2 (2025).
[4] A. J. Baltz, Y. Gorbunov, S. R. Klein, and J. Nystrand, Phys. Rev. C **80**, 044902 (2009).
[5] M. Herman, R. Capote, B. Carlson, P. Obložinský, M. Sin, A. Trkov, H. Wienke, and V. Zerkin, Nucl. Data Sheets **108**, 2655 (2007).
[6] R. J. Charity, Phys. Rev. C **82**, 014610 (2010).
[7] D. Lacroix, A. Van Lauwe, and D. Durand, Phys. Rev. C **69**, 054604 (2004).
[8] S. Acharya, *et al.*, Phys. Rev. C **111**, 054906 (2025).
[9] J. D. Jackson, *Classical Electrodynamics* (John Wiley & Sons, New York, 1972).
[10] I. A. Pshenichnov, I. N. Mishustin, J. P. Bondorf, A. S. Botvina, and A. S. Iljinov, Phys. Rev. C **60**, 044901 (1999).
[11] O. Buss, T. Gaitanos, K. Gallmeister, H. van Hees, M. Kaskulov, O. Lalakulich, T. L. A. Larionov, J. Weil, and U. Mosel, Phys. Rep. **512**, 1 (2012).
[12] L. A. Sopln, R. C. Fernndez, J. Gustafson, D. Quinn, and S. Yadav, Comput. Phys. Commun. **311**, 109553 (2025).
[13] R. A. Yassine, *et al.* (HADES Collaboration), Phys. Rev. C **108**, 064902 (2023).
[14] R. A. Yassine, *et al.* (HADES Collaboration), Eur. Phys. J. A **60**, 18 (2024).
[15] A. B. Larionov, T. Gaitanos, and U. Mosel, Phys. Rev. C **85**, 024614 (2012).

[16] V. F. Weisskopf and D. H. Ewing, Phys. Rev. **57**, 472 (1940).
[17] S. Furihata, Nucl. Instrum. Methods B **171**, 251 (2000).
[18] S. Furihata and T. Nakamura, J. Nucl. Sci. Technol. **39**, 758 (2002).
[19] A. Gilbert and A. G. W. Cameron, Can. J. Phys. **43**, 1446 (1965).
[20] R. E. Prael and H. Liechtenstein, User guide to LCS: The LAHET code system, Los Alamos National Laboratory, 1989.
[21] M. Ciemała, *et al.*, Phys. Rev. C **91**, 054313 (2015).
[22] W. Hauser and H. Feshbach, Phys. Rev. **87**, 366 (1952).
[23] P. Möller, J. R. Nix, W. D. Myers, and W. J. Świątecki, At. Data Nucl. Data Tables **59**, 185 (1995).
[24] J. Ahrens, H. Borchert, K. H. Czock, H. B. Eppler, H. Grimm, H. Gundrum, M. Kröning, P. Riehn, G. Sita Ram, A. Zieger, and B. Ziegler, Nucl. Phys. A **251**, 479 (1975).
[25] C. Guaraldo, V. Lucherini, E. De Sanctis, A. Iljinov, M. Mebel, and S. Lo Nigro, Il Nuovo Cimento A **103**, 607 (1990).
[26] K. Pysz, Phys. Rev. C **91**, 011602(R) (2015).
[27] A. Budzanowski, *et al.*, Phys. Rev. C **82**, 034605 (2010).
[28] A. Budzanowski, *et al.*, Phys. Rev. C **80**, 054604 (2009).
[29] M. Fidelus, *et al.*, Phys. Rev. C **89**, 054617 (2014).
[30] A. Leprêtre, H. Beil, R. Bergere, P. Carlos, J. Fagot, A. Veyssiere, J. Ahrens, P. Axel, and U. Kneissl, Phys. Lett. B **79**, 43 (1978).
[31] A. Leprêtre, H. Beil, R. Bergère, P. Carlos, J. Fagot, A. De Miniac, and A. Veyssière, Nucl. Phys. A **367**, 237 (1981).
[32] A. Leprêtre, H. Beil, R. Bergère, P. Carlos, J. Fagot, A. Veyssière, and I. Halpern, Nucl. Phys. A **390**, 221 (1982).
[33] M. Broz, J. G. Contreras, J. D. Tapia Takaki, Comput. Phys. Commun. **253**, 107181 (2020).
[34] I. A. Pshenichnov, Phys. Part. Nuclei **42**, 215 (2011).
[35] C. Y. Fu, T. A. Gabriel, and R. A. Lillie, *Proceedings of the Third Specialists Meeting on SATIF-3 Shielding Aspects of Accelerators, Targets and Irradiation Facilities, Tohoku University, Sendai, Japan, 1997*, OECD/NEA (OECD Publishing, Paris, 1998), pp. 49–60.
[36] D. P. Watts, I. J. D. MacGregor, J. Ahrens, J. R. M. Annand, R. Beck, D. Branford, P. Grabmayr, S. J. Hall, P. D. Harty, T. Hehl, J. D. Kellie, T. Lamparter, M. Liang, J. A. MacKenzie, S. McAllister, J. C. McGeorge, R. O. Owens, M. Sauer, R. Schneider, G. J. Wagner, *et al.*, Phys. Rev. C **62**, 014616 (2000).
[37] R. Williams, Ph.D. thesis, University of York, Department of Physics, Engineering and Technology, 2024.
[38] C. Bochna, *et al.*, Phys. Rev. Lett. **81**, 4576 (1998).
[39] M. Kłusek-Gawenda, M. Ciemała, W. Schäfer, and A. Szczurek, Phys. Rev. C **89**, 054907 (2014).
[40] J. Dudek and T. Werner, J. Phys. G **4**, 1543 (1978).
[41] J. Dudek, A. Majhofer, J. Skalski, T. Werner, S. Cwiok, and W. Nazarewicz, J. Phys. G **5**, 1359 (1979).
[42] J. Dudek, W. Nazarewicz, and T. Werner, Nucl. Phys. A **341**, 253 (1980).
[43] J. Dudek, Z. Szymański, and T. Werner, Phys. Rev. C **23**, 920 (1981).
[44] S. Cwiok, J. Dudek, W. Nazarewicz, J. Skalski, and T. Werner, Comput. Phys. Commun. **46**, 379 (1987).
[45] H. Dahmen, F. Dreyer, J. Staude, and H. Thies, Nucl. Phys. A **164**, 140 (1971).
[46] T. Sato and T. S. H. Lee, Phys. Rev. C **54**, 2660 (1996).
[47] A. Donnachie and P. Landshoff, Phys. Lett. B **478**, 146 (2000).
[48] A. Bolz, C. Ewerz, M. Maniatis, O. Nachtmann, M. Sauter, and A. Schöning, J. High Energy Phys. 01 (2015) 151.
[49] A. Cisek, W. Schäfer, and A. Szczurek, Phys. Lett. B **836**, 137595 (2023).
[50] L. Frankfurt, V. Guzey, M. Strikman, and M. Zhalov, Phys. Lett. B **752**, 51 (2016).
[51] G. Ingelman, A. Edin, and J. Rathsman, Comput. Phys. Commun. **101**, 108 (1997).
[52] H. Holtmann, G. Levman, N. Nikolaev, A. Szczurek, and J. Speth, Phys. Lett. B **338**, 363 (1994).
[53] A. Szczurek, N. Nikolaev, and J. Speth, Phys. Lett. B **428**, 383 (1998).
[54] A. Szczurek, G. D. Bosveld, and A. E. Dieperink, Nucl. Phys. A **595**, 307 (1995).
[55] A. Szczurek and J. Speth, Nucl. Phys. A **555**, 249 (1993).
[56] H. Holtmann, A. Szczurek, and J. Speth, Nucl. Phys. A **596**, 631 (1996).
[57] A. Szczurek, A. J. Buchmann, and A. Faessler, J. Phys. G: Nucl. Part. Phys. **22**, 1741 (1996).
[58] T. E. O. Ericson and W. Weise, *Pions and Nuclei* (Clarendon Press, Oxford, 1988).
[59] O. Hen, *et al.*, arXiv:2009.09617.
[60] J. Ryckebusch, W. Cosyn, S. Stevens, C. Casert, and J. Nys, Phys. Lett. B **792**, 21 (2019).
[61] M. Duer, *et al.*, Phys. Rev. Lett. **122**, 172502 (2019).